運輸省港湾技術研究所

港湾技術研究所報告

REPORT OF THE PORT AND HARBOUR RESEARCH INSTITUTE

MINISTRY OF TRANSPORT

VOL. 14 NO. 3 SEPT. 1975

NAGASE, YOKOSUKA, JAPAN

港湾技術研究所報告 (REPORT OF P.H.R.I.)
第14巻 第3号 (Vol. 14, No. 3), 1975年9月 (Sept. 1975)

目 次 (CONTENTS)

REPORT OF THE PORT AND
HARBOUR RESEARCH INSTITUTE
Vol. 14 No. 3 (Sept. 1975)

1. Influence of the clearance between bed and mouth sucking a solid body

Yoshikuni OKAYAMA*
Tokuji YAGI**
Yoshihiro SATO***
Masaru SAITO***

Synopsis

In order to investigate the influence of the clearance between the ground and the suction mouth for the lift of the solid body, the room experiment was conducted by using the model bed and the circular suction mouth.

The change of the lift was obtained by means of measuring the tension for the solid sphere laid on the bed.

The drag coefficient of the sphere increases initially due to the hasty increase of the velocity at the inlet of the mouth and gradually approach the constant value. The similar flow around the suction mouth is given by adopting dimentionless parameter and its general relation is expressed as follows:

$$\overset{*}{C}_D = k_d \overset{*}{R}_D^{\delta}$$

where

$$\overset{*}{C}_D = \overset{*}{T} / \left\{ \frac{\rho}{2} (\xi^{3.52} V_p)^2 D_s^2 \right\}$$

$$\overset{*}{R}_D = / \nu (D_s \xi^{3.52} V_p)$$

The numerical calculation utilized Finite Difference Method was carried out for potential flow in order to examine the similitude of the flow. As the result of this calculation the relation of the similitude is given approximately by dimentionless parameter derived for the experimental data.

Further, it is revealed that this parameter, $\xi^{3.52}$, decides absolute velocity at arbitrary point of the flow field excepting back area of the sphere.

* Senior Research Engineer, Machinery Division
** Chief of the Hydraulic Transportation Laboratory, Machinery Division
*** Member of the Hydraulic Transportation Laboratory, Machinery Division

港湾技術研究所報告
第 14 巻 第 3 号 (1975.9)

1. 吸込間隙の影響を受ける固体の吸込力について

岡山義邦*
八木得次**
佐藤義博***
斉藤　勝***

要　旨

海底の固体を吸引する場合，海底地盤と吸込マウスとの間隙の変化によって，その吸込力がどのように変るかという点について調べるために，模擬海底ベッドと円形マウスを使って室内実験を行った。

この結果，間隙を小さくすると円形マウスの入口に急激な速度の上昇が得られ抗力係数が増加してゆくが，最終的には，一定の値に漸近することが判った。また間隙の変化による吸込口の相似な流れは，無次元パラメータ $\xi^{3.52}$ を用いることにより与えられ，その一般的関係は次式のように表わされる。

$$\overset{*}{C}_D = k_d \overset{*}{R}_D^{\beta}$$

ここで

$$\overset{*}{C}_D = \overset{*}{T}\Big/\left\{\frac{\rho}{2}(\xi^{3.52}V_p)^2 D_s^2\right\}$$

$$\overset{*}{R}_D = \nu/(D_s\xi^{3.52}V_p)$$

この間隙の変化による吸込力の相似性を検討するために，ポテンシャル流に対して差分近似式を用いた数値計算を行った。この結果をひとつの実験データとして相似関係を調べると，実験値に対して得られたパラメータで近似的に整理されること，そしてこのパラメータ $\xi^{3.52}$ は，球の背部を除いた吸込みの場の絶対速度を決定するものでもあるということが判った。

*　機材部　主任研究官
**　機材部　流体輸送研究室長
***　機材部　流体輸送研究室

Contents

1. Introduction

The researches on the problem dealed with a clearance between sea bed and suction mouth have not been carried out because that the influences by the clearance was not significant in ordinary port and harbour construction. However, judging from the results[1)2)] concerning suction hopper dredger the influence of clearance becomes to be considerable factor in case of dredging with auxiliary device such as teeth.

Further, as far as dredging of hard rock by electro-magnetic wave is concerned, the clearance between suction mouth and rock surface is restricted. Therefore in this case the effective inlet flow enough for gathering crushed rock must be considered to the restricted clearance. In addition to these matters this problem should require more consideration also in deep sea dredging by air lift system and in the treatment of solid disposals.

In order to grasp the influence of the clearance the room experiment with model sea bed was conducted and the drag force of sphere by the flow absorbed into suction mouth was measured. Moreover the numerical calculation by Finite Difference Method (F.D.M.) was conducted in order to investigate the similarlity of the flow to the various clearances.

This paper presents the details on the aforementioned experimental and theoretical investigation.

2. Experimental Instruments and Procedure

2.1. Experimental Instruments

The aspect of experimental facilities is shown in Fig. 2-1.

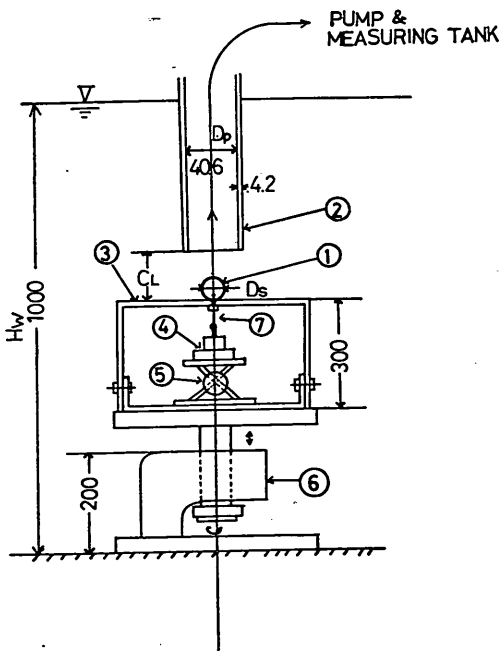

Fig. 2-1 Shematic description of experimental system

The dimension of the water pool used for this experiment is 1.0 m in depth, 1.5 m in width and 5 m in length. The flow around the sphere is given by the suction pump of which specifications are followings.

Caliber.....1 1/2 inch
Delivery Quantity.....0.2 m^3/min
Total Head.....11.5 m

The model bed (3) made of stainless steel has the breadth of 400×400mm and installes the small pipe which protects flactuation of the sphere in the horizontal direction. The inner diameter of this pipe is 1.0 mm and fine stainless thread (7) fixed at the center of the sphere (1) is connected to the tension meter (4) through the pipe. This tension meter is placed on the laboratry jack (5) which adjusts looseness of the stainless thread. The clearance between the suction mouth and the bed, C_L, is changed by using the jack (6). The dimension of the sphere and the suction pipe is

D_s=31.4 mm
D_p=40.6 mm (thickness t=4.2 mm)

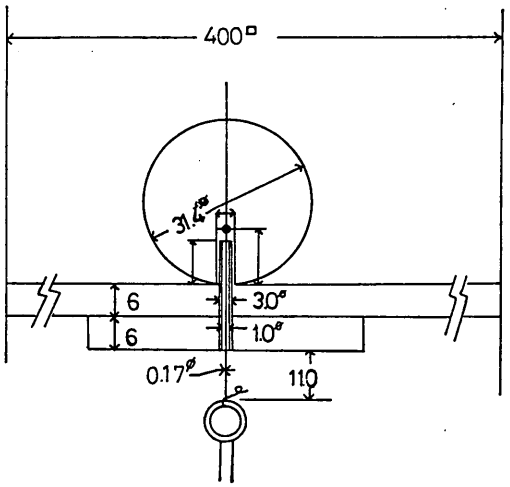

Fig. 2-2 Connection of sphere and tension meter with stainless thread

Fig. 2-2 show the details of the connected part between the sphere and the tension meter. The capacity of this tension meter is 1,000 g (max) and, then, the amount of strain shows 1,070 micro strain. There is no influence of water pressure to this tension meter because water pressure affects to the diaphragm upward and downward. The Photo. 1, 2 show the model bed and tension meter respectively. The sphere is acryl ball and its specific weight is 1.185.

2.2. Experimental procedure

Firstly the clearance C_L was set by using the jack (6) on the condition that the stainless thread was loosen. Then after this thread was adjusted in order to obtaine accurate tension, the pump was driven. The flow velocity was varied with the opening ratio of the valve installed at the delivery pipe and the flow rate was measured by the measuring tank placed bellow the delivery pipe. Tension and vaccum pressure were simultaneously recorded on the oscillograph.

As the clearance C_L change finely during the experiment, the clearance C_L was strictly measured before and after in the test period. Judging from this measuring there were little difference between two clearances.

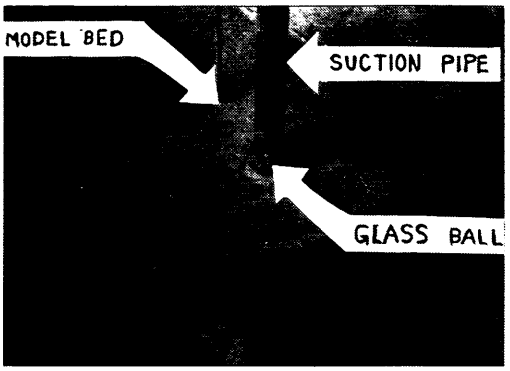

Photo. 1 Model sea bed

Photo. 2 Tension meter

The procedure mentioned above is one experiment for one condition decided by the clearance C_L and it was repeated for 15 kinds of clearance. Table 1 shows C_L for each test. In this table the number of times, N, doesn't mean continuous experiment. Though there exists a little difference in data for same clearance and flow rate, this can be thought the adjustment of stainless thread differed finely in each time.

Table 1 Clearance for each experiment

Case No.	C_L (mm)	Number of time
1	53.0	2
2	51.0	2
3	50.0	3
4	49.0	2
5	47.0	3
6	46.0	1
7	45.0	2
8	44.5	1
9	44.0	2
10	43.0	1
11	42.5	3
12	42.0	1
13	41.0	1
14	40.0	1
15	37.5	2

The water level H_w was kept constant during the whole experiments and didn't decrease in the period of measuring of flow rate due to the relatively wide water pool.

3. Numerical Calculation of Drag Force

The calculation was conducted on the assumption that the flow is axially symmetric, incompressible and potential flow. The basic equation on potential flow is substituted approximatery for finite difference on arbitrary point in the flow field. The flow is decided by solving the approximate formula so that it is satisfied in all points. On boundary the known stream function is given as boundary condition. The dimensions of the sphere and the suction pipe are

$$D_s=31.0\,\text{mm}$$
$$D_p=40.0\,\text{mm}\ \ (\text{thickness}\ t=4.2\,\text{mm})$$

Basic equation for the axially symmetric, incompressible and potential flow is obtained as followings. We let suppose ring-shaped space in coordinate system(r, z) as shown in Fig. 3-1, where u and w are velocity component in r and z direction respectively.

The amount of volume expressed by (1) goes out per unit time through the perpendicular surface to z axis.

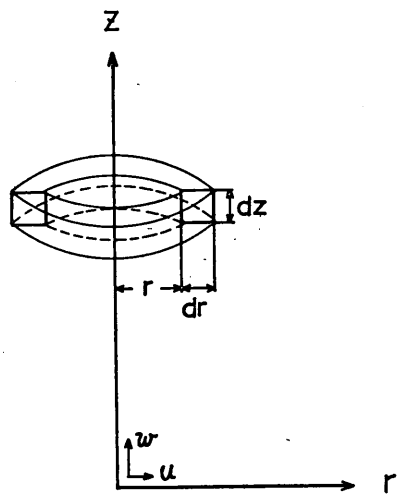

Fig. 3-1 Axially symmetric coordinate

$$\frac{\partial}{\partial z}(w2\pi r\cdot dr)dz \qquad (1)$$

And that expressed by (2) goes out through the perpendicular surface to r axis.

$$\frac{\partial}{\partial z}(u2\pi rdz)dr \qquad (2)$$

The sum of these two values is zero according to the law of conservation of mass. That is

$$\frac{\partial}{\partial z}(w2\pi dr)dz+\frac{\partial}{\partial r}(u2\pi rdz)dr=0$$

Thus,

$$\frac{\partial}{\partial z}(wr)+\frac{\partial}{\partial r}(ur)=0 \tag{3}$$

The relation (3) is necessary and sufficient condition for that $(wrdr-urdz)$ is total differential. This total differential is represented by $d\psi$.

$$d\psi=wrdr-urdz \tag{4}$$

Therefore,

$$u=-\frac{1}{r}\frac{\partial\psi}{\partial z}$$
$$w=\frac{1}{r}\frac{\partial\psi}{\partial r} \tag{5}$$

where ψ is named Stokes' stream function[3] for axially symmetric flow. The basic equation (6) with condition for no rotation, $\frac{\partial w}{\partial r}-\frac{\partial u}{\partial z}=0$, is obtained by equation(5).

$$\frac{\partial^2\psi}{\partial r^2}-\frac{1}{r}\frac{\partial\psi}{\partial r}+\frac{\partial^2\psi}{\partial z^2}=0 \tag{6}$$

Equation (6) is expressed approximately as equation (7) by using the stream function at point 0 and other four points around it in Fig. 3-2.

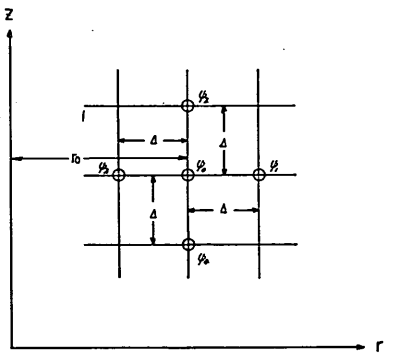

Fig. 3-2 Partition by square mesh

$$\frac{\partial^2\psi}{\partial r^2}-\frac{1}{r}\frac{\partial\psi}{\partial r}+\frac{\partial^2\psi}{\partial z^2}\simeq\frac{1}{\Delta^2}\left[\psi_1+\psi_2+\psi_3+\psi_4-4\psi_0-\frac{\psi_1-\psi_3}{2f}\right] \tag{7}$$

where,

$$f=r_0/\Delta$$

Thus the relationship (8) can be obtained from Eq. (6) in the flow field as shown in Fig. 3-2.

$$\psi_1+\psi_2+\psi_3+\psi_4-4\psi_0-\frac{\psi_1-\psi_3}{2f}\simeq 0 \tag{8}$$

Therefore, when the stream functions on the whole points are calculated so that the

left side of the relationship (8) for each points may close to zero, the stream function for every points satisfy equation (3) approximately. Such calculation was conducted by means of Relaxation Method[4].

3.1. Partition of flow field by grid lines

The flow field as shown in Fig. 3-3 is divided into square parts by many grid lines. The mesh is fine for the part in which the flow changes quickly and rough for the outside part. Though such a different partition may have some influences on the result of the calculation by using Finite Difference Method, this matter is not considered in this paper.

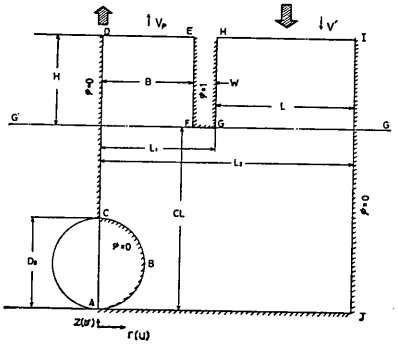

Fig. 3-3 Schem of flow field

Now, the center line can be treated as boundary under potential flow. Further, the annular outside wall differing from one of the experiment is used for this calculation on account of the convenience for the decision of boundary condition.
The Photo. (3) shows the flow field devided into fine mesh.

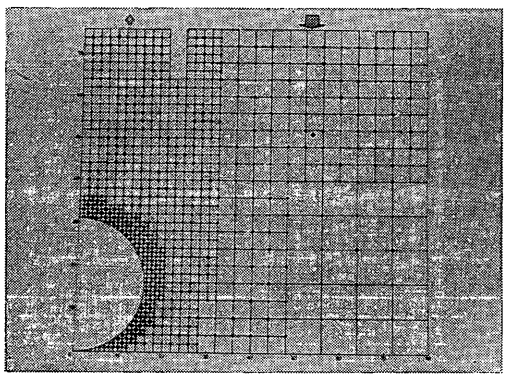

Photo. 3 Partition of flow field by square mesh

3.2. Boundary condition

If the flow on D-E and H-I is assumed to be uniform flow of which velocity is V_p and V' respectively, $u=0$ and $w=V_p$ are obtained on D-E.
From equation (5), we have

$$V_p=\frac{1}{r}\frac{\partial\psi}{\partial r} \qquad (9)$$

Hence, ψ is obtained by integrating equation (9).

$$\phi=\frac{V_p}{2}r^2+C_1 \tag{10}$$

Equation (10) is expressed in non-dimensional expression as follows:

$$\overset{*}{\phi}=\overset{*}{r}^2+K \tag{11}$$

where,

$$\overset{*}{r}=r/B,\ \phi=\phi/\frac{V_p}{2}B^2$$

If we choose the condition of $\overset{*}{\phi}=0$ on I-J-A-B-C-D and $\overset{*}{\phi}=1$ on E-F-G-H, K must be zero.

Therefore non-dimensoonal stream function, $\overset{*}{\phi}$, on D-E is decided as follows:

$$\overset{*}{\phi}=\overset{*}{r}^2 \tag{12}$$

As far as the boundary H-I is concerned, the velocity, V', on H-I is expressed by V_p due to the condition of the continuity.
That is

$$V'=\frac{B^2}{L_2^2-L_1^2}V_p \tag{13}$$

Hence, as shown in equation (14) stream function on H-I is derived with same procedure for equation (12).

$$\overset{*}{\phi}=\frac{\overset{*}{L}-\overset{*}{r}^2}{\overset{*}{L}_2^2-\overset{*}{L}_1^2} \tag{14}$$

where,

$$\overset{*}{L}_2=L_2/B,\ \overset{*}{L}_1=L_1/B$$

Thus, the boundary condition is obtained as follows:

$$\begin{aligned}
&\phi=0 && \text{.....on I-J-A-B-C-D}\\
&\phi=1 && \text{.....on E-F-G-H}\\
&\phi=r^2 && \text{.....on D-E}\\
&\phi=(L_2^2-r^2)/(L_2^2-L_2^2) && \text{.....on H-I}
\end{aligned} \tag{15}$$

where all values are written in the original expression, but now they are non-dimensional value and it is the same in the following procedures.

3.3. Calculation by Relaxation Method

3.3.1. Gradual formula

(a) Case for square mesh

We now let derive the gradual formula for the point 0 in Fig. 3-2. By putting the error, ε_r, into the relation (8), equation (16) is obtained.

$$\phi_1+\phi_2+\phi_3+\phi_4-4\phi_0-\frac{\phi_1-\phi_3}{2f}=\varepsilon_r \tag{16}$$

If we correct ψ_0 so that the error may close to zero, and the addition is denoted by ε, equation (16) becomes

$$\psi_1+\psi_2+\psi_3+\psi_4-4(\psi_0+\varepsilon)-\frac{\psi_1-\psi_3}{2f}=0 \tag{17}$$

Hence,

$$\varepsilon=\frac{1}{4}\left[\psi_1+\psi_2+\psi_3+\psi_4-\frac{\psi_1-\psi_3}{2f}\right]-\psi_0 \tag{18}$$

is obtained.

Generally speaking, the vaue corrected on the value of ψ_0 is expressed as equation (19) by using the calculation coefficient, k_c.

$$\psi_0+k\varepsilon=\psi_0+\frac{k}{4}\left[\psi_1+\psi_2+\psi_3+\psi_4-\frac{\psi_1-\psi_3}{2f}\right]-k\psi_0 \tag{19}$$

Equation (19) is extended to the general gradual equation as follows:

$$\psi_0^{(J+1)}=\frac{k_c}{4}\left[\psi_1^{(J)}+\psi_2^{(J)}+\psi_3^{(J)}+\psi_4^{(J)}-\frac{\psi_1^{(J)}-\psi_3^{(J)}}{2f}\right]+(1-k_c)\psi_0^{(J)} \tag{20}$$

As in this paper the calculation was carried out for $k_c=1$, equation (20) becomes

$$\psi_0^{(J+1)}=\frac{1}{4}\left[\psi_1^{(J)}+\psi_2^{(J)}+\psi_3^{(J)}+\psi_4^{(J)}-\frac{\psi_1^{(J)}-\psi_3^{(J)}}{2f}\right] \tag{20}'$$

(b) Case for unequal square mesh

The area near to the surface of the sphere has the unequal mesh as shown in Fig. 3-4.

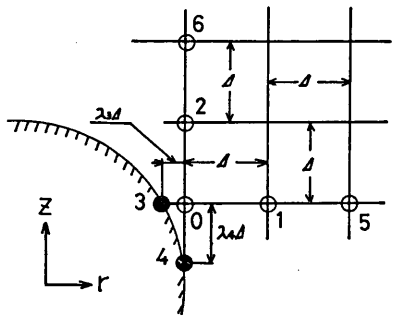

Fig. 3-4 Partition by unequal square mesh

The gradual formula for such mesh is derived as the followings.

We now let investigate the order of the error in the finite difference used in equation (8).

This can be understood by considering the Taylor's expansion on the stream function, ψ. For example,

$$\left(\frac{\delta^2\psi}{\delta r^2}\right)_0=\frac{1}{\Delta^2}\{\psi_1+\psi_3-2\psi_0\} \tag{21}$$

is obtained in Fig. 3-2. Now, if Tailar's expansion is applied to the right side of equation (21), equation (22) is developed as follows:

$$\begin{aligned}\left(\frac{\delta^2\psi}{\partial r^2}\right)_0 &= \frac{1}{\Delta^2}\{\psi(r_0+\Delta)+\psi(r_0-\Delta)-2\psi(r_0)\} \\ &= \frac{1}{\Delta^2}\left[\left\{\psi(r_0)+\frac{\Delta}{1!}\dot{\psi}(r_0)+\frac{\Delta^2}{2!}\ddot{\psi}(r_0)+\frac{\Delta^{3(3)}}{3!}\dot{\psi}(r_0)+\cdots\right\}\right. \\ &\quad \left.+\left\{\psi(r_0)-\frac{\Delta}{1!}\dot{\psi}(r_0)+\frac{\Delta^2}{2!}\ddot{\psi}(r_0)-\frac{\Delta^{3(3)}}{3!}\dot{\psi}(r_0)+\cdots\right\}-2\psi(r_0)\right] \\ &= \ddot{\psi}(r_0)+2\left[\frac{\overset{(4)}{\psi}(r_0)}{4!}\Delta^2+\frac{\overset{(6)}{\psi}(r_0)}{6!}\Delta^3+\cdots\right] \end{aligned} \tag{22}$$

As $\left(\frac{\partial^2\psi}{\partial r^2}\right)_0$ is substituted for $\ddot{\psi}(r_0)$ in this calculation, the order of the error is Δ^2. Similarly, another differences $\left(\frac{\partial^2\psi}{\delta z^2}\right)_0$ and $\frac{1}{r_0}\left(\frac{\delta\psi}{\delta r}\right)_0$ have the order of Δ^2 for partial differential $\left(\frac{\partial^2\psi}{\partial z^2}\right)_0$ and $\frac{1}{r_0}\left(\frac{\partial\psi}{\partial r}\right)_0$ respectively.
Therefore, the order of the approximate error must be the order of Δ^2.

Let us utilize Tailor's expansion on the stream function ψ_1, ψ_3 around the point 0 in the direction of r-axis. And if we omitt the terms higher than third order of Δ,

$$\psi_1=\psi_0+\frac{\Delta\dot{\psi}_0}{1!}+\frac{\Delta^2}{2!}\ddot{\psi}_0 \tag{23}$$

$$\psi_3=\psi_0-\frac{\lambda_3\Delta\dot{\psi}_3}{1!}+\frac{(\lambda_3\Delta)^2}{2!}\ddot{\psi}_0 \tag{24}$$

are obtained. If we eliminate $\ddot{\psi}_0$ from equation (23) and (24), the value of $\left(\frac{\delta\psi}{\delta r}\right)_0$ is expressed as

$$\left(\frac{\delta\psi}{\delta r}\right)_0=\frac{1}{\Delta}\left[\frac{1}{1+\lambda_3}\frac{\psi_0-\psi_3}{\lambda_3}+\frac{\lambda_3}{1+\lambda_3}(\psi_1-\psi_0)\right] \tag{25}$$

Thus,

$$\frac{1}{r_0}\left(\frac{\delta\psi}{\partial r}\right)_0=\frac{1}{\Delta^2}\frac{1}{(1+\lambda_3)f}\left\{\frac{\psi_0-\psi_3}{\lambda_3}+\lambda_3(\psi_1-\psi_0)\right\} \tag{26}$$

is obtained.

Similarly, the difference $\left(\frac{\delta^2\psi}{\delta r^2}\right)$ in Fig. 3-4 is obtained as follows:

$$\psi_3=\psi_0-\frac{\lambda_3\Delta}{1!}\dot{\psi}_0+\frac{(\lambda_3\Delta)^2}{2!}\ddot{\psi}_0-\frac{(\lambda_3\Delta)^{3(3)}}{3!}\dot{\psi}_0 \tag{27}$$

$$\psi_1=\psi_0+\frac{\Delta}{1!}\dot{\psi}_0+\frac{\Delta^2}{2!}\ddot{\psi}_0+\frac{\Delta^{3(3)}}{3!}\dot{\psi}_0 \tag{28}$$

$$\psi_5=\psi_0+\frac{2\Delta}{1!}\dot{\psi}_0+\frac{(2\Delta)^2}{2!}\ddot{\psi}_0+\frac{(2\Delta)^{3(3)}}{3!}\dot{\psi}_0 \tag{29}$$

By eliminating $\dot{\psi}_0$ and $\overset{(3)}{\psi}_0$ from equation (27), (28), (29), we get

$$\left(\frac{\delta^2\psi}{\delta r^2}\right)_0=\frac{1}{\Delta^2}\left[\frac{2(2-\lambda_3)}{1+\lambda_3}\psi_1-\frac{1-\lambda_3}{2+\lambda_3}\psi_5+\frac{6\psi_3}{\lambda_3(1+\lambda_3)(2+\lambda_3)}-\frac{3-\lambda_3}{\lambda_3}\psi_0\right] \tag{30}$$

Similarly, we get the following equation.

$$\left(\frac{\delta^2\psi}{\delta z^2}\right)_0=\frac{1}{\Delta^2}\left[\frac{2(2-\lambda_4)}{1+\lambda_4}\psi_2-\frac{1-\lambda_4}{2+\lambda_4}\psi_6+\frac{6\psi_4}{\lambda_4(1+\lambda_4)(2+\lambda_4)}-\frac{3-\lambda_4}{\lambda_4}\psi_0\right] \tag{31}$$

Hence,

$$\begin{aligned}
&\left(\frac{\delta^2\psi}{\delta r^2}+\frac{\delta^2\psi}{\delta z^2}-\frac{1}{r}\frac{\delta\psi}{\delta r}\right)_0\\
&=\frac{1}{\Delta^2}\left[\frac{2(2-\lambda_3)}{1+\lambda_3}\psi_1+\frac{2(2-\lambda_4)}{1+\lambda_4}\psi_2+\frac{6\psi_3}{\lambda_3(1+\lambda_3)(2+\lambda_3)}+\frac{6\psi_4}{\lambda_4(1+\lambda_4)(2+\lambda_4)}\right.\\
&\quad\left.-\frac{1-\lambda_3}{2+\lambda_3}\psi_5-\frac{1-\lambda_4}{2+\lambda_4}\psi_6-\left(\frac{3-\lambda_3}{\lambda_3}-\frac{3-\lambda_4}{\lambda_4}\right)\psi_0-\frac{1}{(1+\lambda_3)f}\left(\frac{\psi_0-\psi_3}{\lambda_3}+\psi_1-\psi_0\right)\right.\\
&=\frac{1}{\Delta^2}\left[\frac{2(2-\lambda_3)}{1+\lambda_3}\psi_1+\frac{2(2-\lambda_4)}{1+\lambda_4}\psi_2+\frac{6\psi_3}{\lambda_3(1+\lambda_3)(2+\lambda_3)}+\frac{6\psi_4}{\lambda_4(1+\lambda_4)(2+\lambda_4)}-\frac{1-\lambda_3}{2+\lambda_3}\psi_5\right.\\
&\quad\left.-\frac{1-\lambda_4}{2+\lambda_4}\psi_6+\frac{\psi_3}{\lambda_3(1+\lambda_3)}-\frac{\psi_1}{(1+\lambda_3)f}-\left\{\frac{1}{(1+\lambda_3)f}\frac{1-\lambda_3}{\lambda_3}+\frac{3-\lambda_3}{\lambda_3}+\frac{3-\lambda_4}{\lambda_4}\right\}\psi_0\right]\\
&=\frac{1}{\Delta^2}(T-K\psi_0)
\end{aligned} \tag{32}$$

where,

$$\begin{aligned}
T&=\frac{2(2-\lambda_3)}{1+\lambda_3}\psi_1+\frac{2(2-\lambda_4)}{1+\lambda_4}\psi_2+\frac{6\psi_3}{\lambda_3(1+\lambda_3)(2-\lambda_3)}+\frac{6\psi_4}{\lambda_2(1+\lambda_4)(2-\lambda_4)}\\
&\quad-\frac{1-\lambda_3}{2+\lambda_3}\psi_5-\frac{1-\lambda_4}{2+\lambda_4}\psi_6+\frac{1}{(1+\lambda_3)f}\left(\frac{\psi_3}{\lambda_3}-\psi_1\right)\\
K&=\frac{1}{(1+\lambda_3)f}\frac{1-\lambda_3}{\lambda_3}+\frac{3-\lambda_3}{\lambda_3}+\frac{3-\lambda_4}{\lambda_4}
\end{aligned}$$

Therefore the gradual formula (33) is derived with the same procedure in equation (20)′.

$$\psi_0^{(J+1)}=T^{(J)}/K^{(J)} \tag{33}$$

In the partition as shown in Fig. 3-5 the stream function can be used only one stream function in the negative-direction of Z. In this case the following finite differences are used for obtaining $\left(\frac{\delta^2\psi}{\delta z^2}\right)_0$.

$$\left(\frac{\delta\psi}{\delta z}\right)_{0+\frac{\lambda_2}{2}\Delta}=\frac{\psi_2-\psi_0}{\lambda_2\Delta}$$

$$\left(\frac{\delta\psi}{\delta z}\right)_{0-\frac{\Delta}{2}}=\frac{\psi_0-\psi_4}{\Delta}$$

Consequently,

$$\left(\frac{\delta^2\psi}{\delta z^2}\right)_0=\frac{1}{\left(\frac{\lambda_2}{2}+\frac{1}{2}\right)\Delta^2}\left\{\frac{\psi_2-\psi_0}{\lambda_2}-(\psi_0-\psi_4)\right\}$$

$$=\frac{2}{\Delta^2(1+\lambda_2)}\left\{\frac{\psi_2-\psi_0}{\lambda_2}-(\psi_0-\psi_4)\right\} \tag{34}$$

is obtained.

The error of equation (34) is expressed as followings by means of the method mentioned previously.

$$\left(\frac{\delta^2\psi}{\delta z^2}\right)_0-\left(\frac{\partial^2\psi}{\partial z^2}\right)$$

$$=-\frac{1}{3}(1-\lambda_2)\Delta\overset{(3)}{\psi}_0+\frac{(1+\lambda_2)^3}{12}\Delta^2\overset{(4)}{\psi}_0\cdots\cdots \tag{35}$$

The order of the error Δ in equation (35) differs from that in equation (22). The difference, however, is ignored in this paper because the flow doesn't change quickly around the area shown in Fig. 3-5.

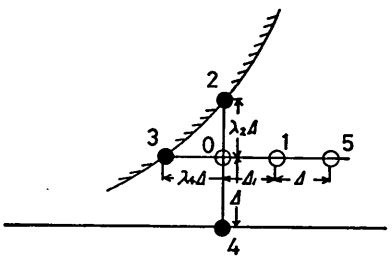

Fig. 3-5 Partition in nook

Therefore, if we use equation (34) in place of $(\delta^2\psi/\delta z^2)_0$ in equation (32), T and K are given as

$$T=\frac{2(2-\lambda_3)}{1+\lambda_3}\psi_1+\frac{2}{\lambda_2(1-\lambda_2)}\psi_2+\frac{6}{\lambda_3(1+\lambda_3)(2+\lambda_3)}\psi_3$$

$$+\frac{2}{1+\lambda_2}\psi_4-\frac{1-\lambda_3}{2+\lambda_3}\psi_5+\frac{1}{(1+\lambda_3)f}\left(\frac{\psi_3}{\lambda_3}-\lambda_3\psi_1\right)$$

$$K=\frac{3-\lambda_3}{\lambda_3}+\frac{2}{\lambda_2}+\frac{1}{(1+\lambda_3)f}\left(\frac{1}{\lambda_3}-\lambda_3\right) \tag{36}$$

And, if we substitute $\lambda=1$ in equation (32) and (36), we have equation (37)

$$T=\psi_1+\psi_2+\psi_3+\psi_4-\frac{1}{2f}(\psi_1-\psi_3)$$

$$K=4 \tag{37}$$

This coincides to the value for square mesh.

Therefore, all gradual formulas are expressed by equation (33).

(C) Case for unequal grid space

In this calculation, 4 kinds of distance Δ between neighbouring grid lines were 1, 2, 4 and 8 mm.

The stream function for the part where distance, Δ, differs at the neighbouring points as shown in Fig. 3-6 was calculated as followings.

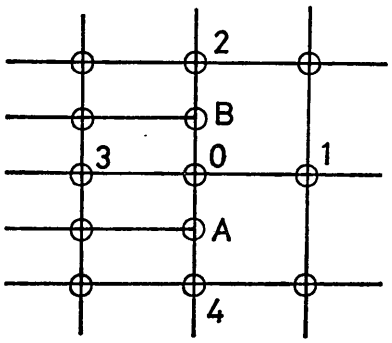

Fig. 3-6 Mesh constituted by different space

The stream function for point 0 was calculated by using four points around it, those are point 1, 2, 3 and 4.

For point A, the arithmetical mean value of the stream function for point 0 and 4 is adopted and for point B, that for point 0 and 2.

3.3.2. Calculation

The calculation for a clearance C_L was repeated until the error became less than the initially fixed value.

The remaining error for the stream function ϕ_0 after the jth calculation is expressed as follows:

$$\varepsilon_{70}^{(j)} = | T^{(j)} - K^{(j)} \phi_0^{(j)} | \tag{38}$$

Equation (38) was calculated for the whole points in each time after the calculation of equation (33). The calculation was ended when ε_{70} became less than the initially fixed value ε_u. All stream functions for that time were adopted as the solutions in this calculation for one clearance C_L. The limit ε_u was choen to be 10^{-5} and the initial value for the whole inner points was adopted to be 0.5.

Further the clearance, C_L, in this calculation was varied in 6 steps and the upper parts from G-G line was expanded according to the increase of C_L.

The Photo. (3) shows the partition by the mesh for the largest clearance C_L.

The dimension of each parts is shown in table (2).

Table 2 Condition of numercal calculation for each clearance

Case No.	C_L (mm)	B (mm)	H (mm)	L_2 (mm)	D_s (mm)	Number of Point Calculated
1	42.0	20.0	14.0	80.0	31.0	723
2	46.0	20.0	14.0	80.0	31.0	769
3	50.0	20.0	14.0	80.0	31.0	815
4	54.0	20.0	14.0	80.0	31.0	861
5	58.0	20.0	14.0	80.0	31.0	907
6	62.0	20.0	14.0	80.0	31.0	953

3.4. Pressure and velocity profiles on a sphere surface

The tangential volocity at the point 0 on the sphere surface in Fig. 3-7 is given by

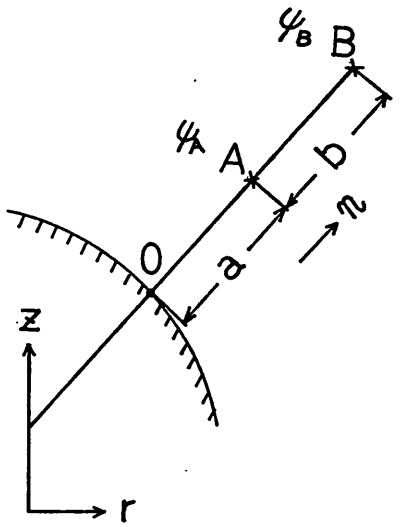

Fig. 3-7 Sketch for calculating tangential velocity on a sphere surface

$$v_t=\frac{1}{r_0}\left(\frac{\partial\psi}{\partial n}\right)_0 \tag{39}$$

where n means the length in the normal.
Now, we let adopt Tailor's expansion and neglect the matter of which the order of partial difference is higher than three.
Thus,

$$\psi_B=\psi_0+(a+b)\left(\frac{\partial\psi}{\partial n}\right)_0+\frac{(a+b)^2}{2}\left(\frac{\partial^2\psi}{\partial n^2}\right)_0 \tag{40}$$

$$\psi_A=\psi_0+a\left(\frac{\partial\psi}{\partial n}\right)_0+\frac{a^2}{2}\left(\frac{\partial^2\psi}{\partial n^2}\right)_0 \tag{41}$$

are obtained.
If the matter concerning $\left(\frac{\partial^2\psi}{\partial n^2}\right)_0$ is eliminated, equation (42) is obtained.

$$\left(\frac{\partial\psi}{\partial n}\right)_0=-\frac{2a+b}{a(a+b)}\psi_0+\frac{a+b}{ab}\psi_A-\frac{a}{b(a+b)}\psi_B \tag{42}$$

And equation (39) can be calculated by using this equation.
Thus, the pressure P_s acting on the surface of the sphere is expressed as follows:

$$P_s=\gamma_w\left\{r(1-\sin\theta)-\frac{v_t^2}{2g}\right\}+P_T \tag{43}$$

where, the pressure at the top of the sphere P_T is chosen as zoro.
Hence, the vertical force T_C affected by P_s in Fig. 3-8 is given as

$$T_C = -2\pi r^2 \int_{-\pi/2}^{\pi/2} P_s \sin\theta \cos\theta d\theta \tag{44}$$

Fig. 3-9 shows the calculated result of v_t and P_s for $V_p=3$ (m/s), and Fig. 3-10 shows $\varepsilon_{r_0}^{(J)}$ given by equation (38) and the number of repetition for each case.

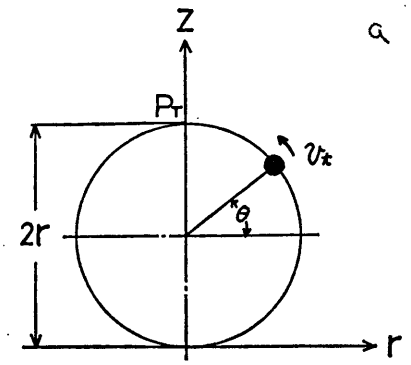

Fig. 3-8 Sketch for calculating pressuredistribution on a sphere

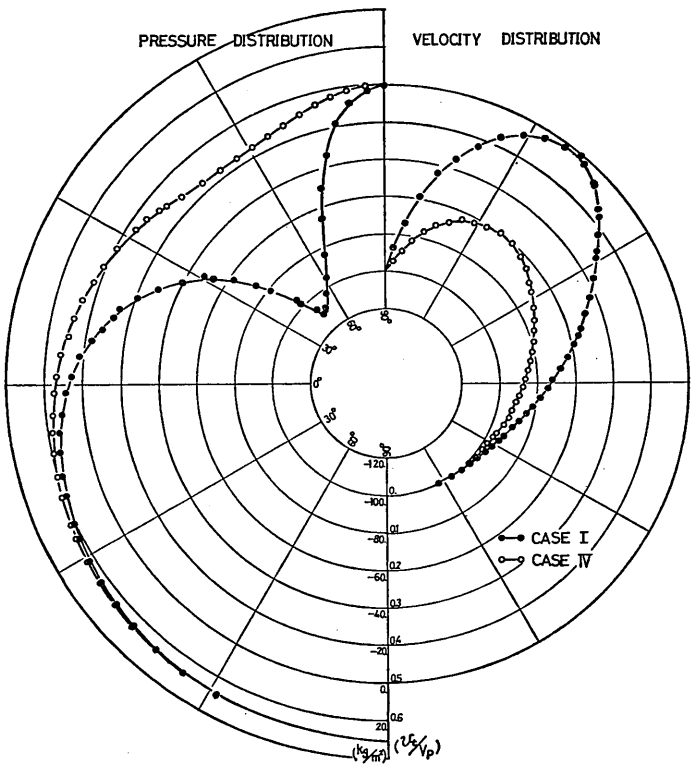

Fig. 3-9 Pressure and velocity profiles on a sphere obtained by calculation

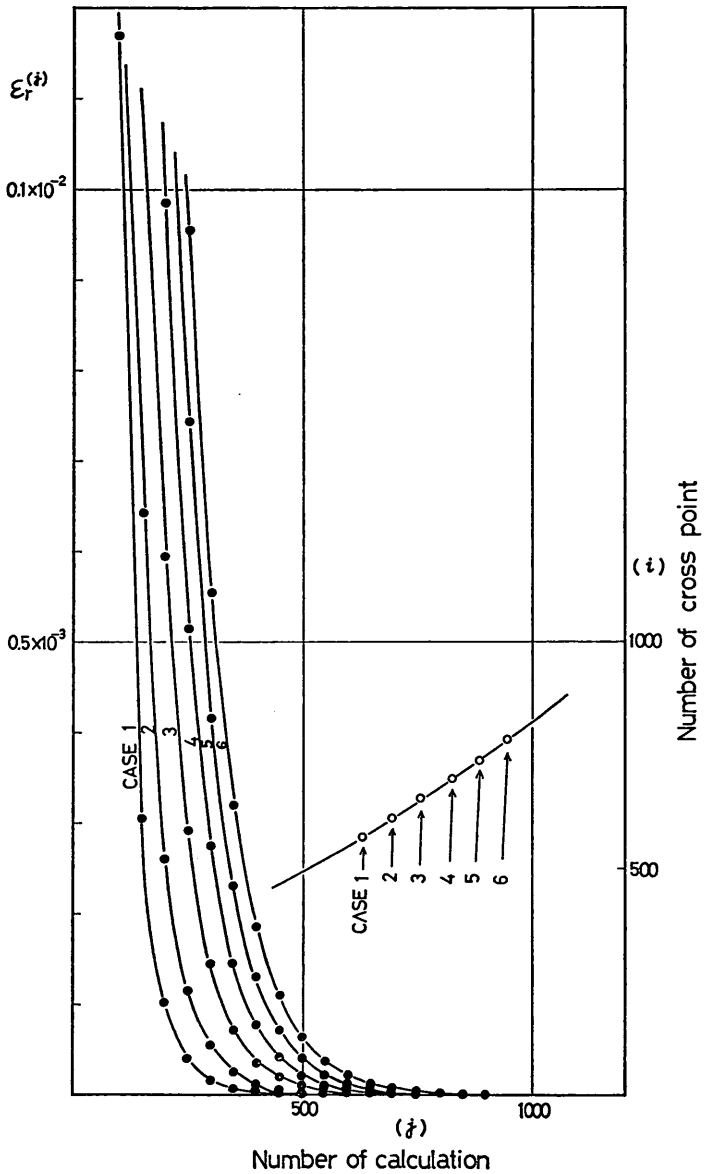

Fig. 3-10 Eroor for the frequency of calculation and the number of calculation at the time error attained the final error

4. Analysis for Experimental and Calculated Results

4.1. Similarlity parameter

Drag force $\overset{*}{T}$ is expressed as equation (45) by using tension T.

$$\overset{*}{T}=T+W_{se}-W_{ce} \tag{45}$$

where W_{se} is the weight of the sphere and W_{ce} is buoyancy acting on the sphere.

Fig. 4-1 shows $\overset{*}{T}$ according to mean flow velocity V_p in pipe. According to this figure the experimental data lay almost on a straight line for each clearance C_L and this fact

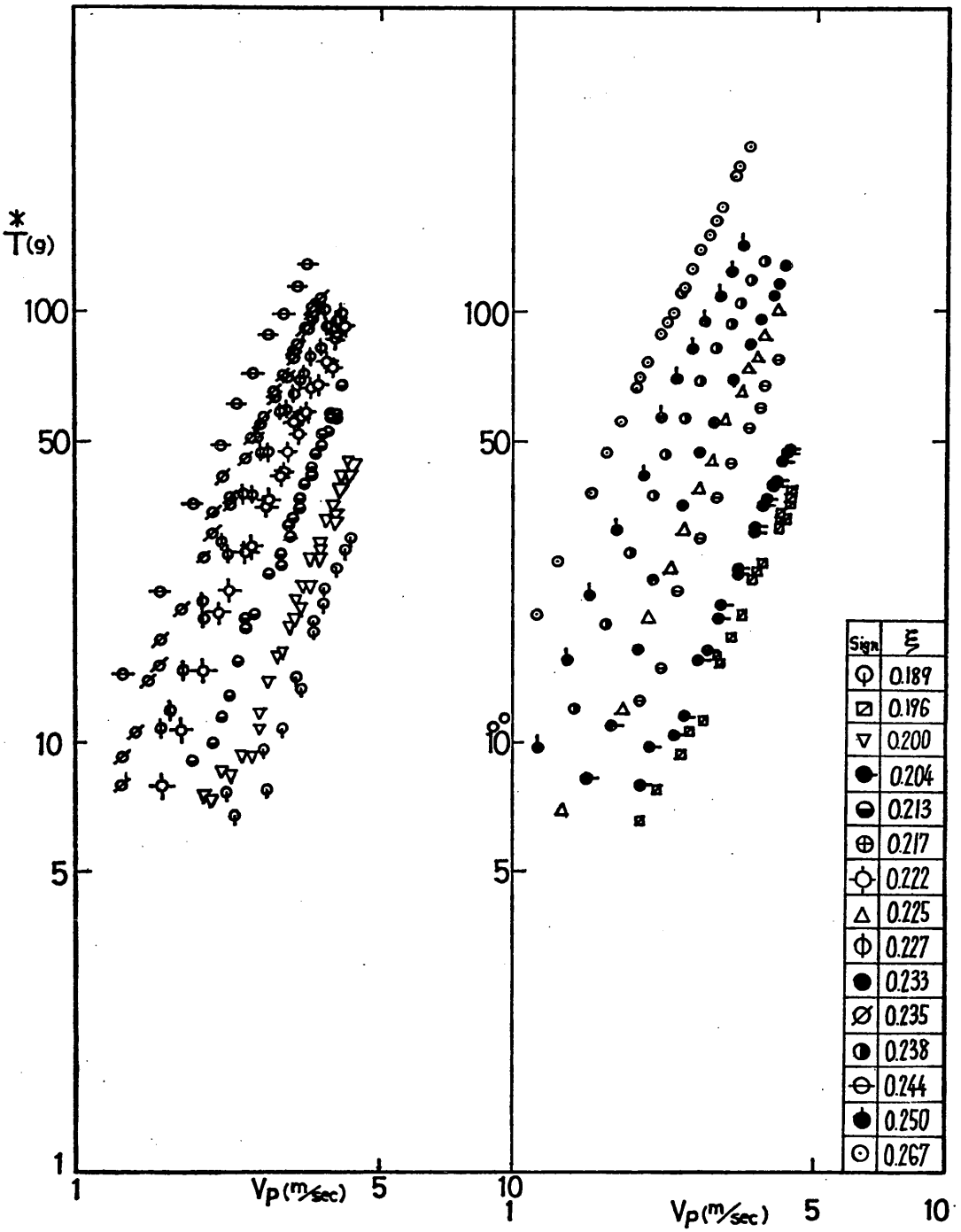

Fig. 4-1 Drag force obtained in experiment versus V_p

reflects the general trend that drag force is proportional to the nth power of velocity. In order to examine these data, let us do dimensional analysis by selecting density of water ρ, diameter of the sphere D_s, mean flow velocity V_p and viscosity of water μ. Thus,

$$\overset{*}{T}=k\rho D_s^2 V_p^2\left(\frac{\mu}{\rho D_s V_p}\right)^{\delta} \tag{46}$$

is obtained, where k is dimensionless coefficient.
As equation (46) doesn't involve the influence by the clearance C_L, k must be coefficient which involves the mattes on the clearance C_L.

If we consider the mean velocity v_m in Fig. 4-2, v_m is written by

$$v_m=\frac{D_p}{4C_L}V_p=\hat{\xi}V_p \tag{47}$$

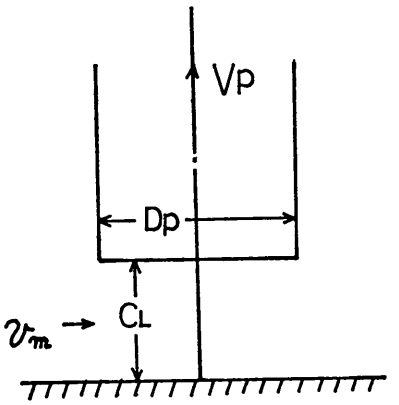

Fig. 4-2 Sketch of flow around suction mouth

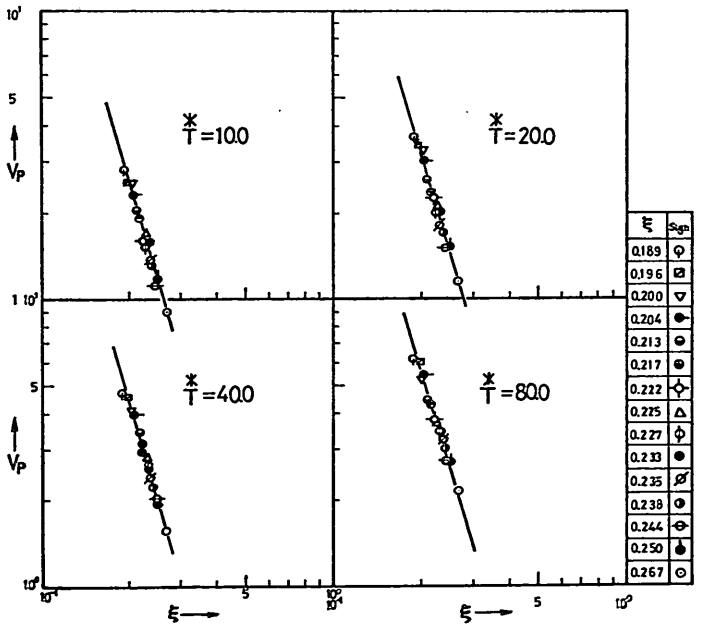

Fig. 4-3 V_p versus dimentionless parameter $\hat{\xi}$ for each drag force

where,

$$\xi=\frac{D_p}{4C_L}$$

Now, if dimensionless parameter ξ is used inplace of k in equation (46), equation (46) is the general equation in which the influence by C_L is deliberated. Thus,

$$\overset{*}{T}=k'\mu^m\rho D_s^2 V_p^2\left(\frac{\mu}{\rho D_s V_p}\right)^\delta \tag{48}$$

is derived.

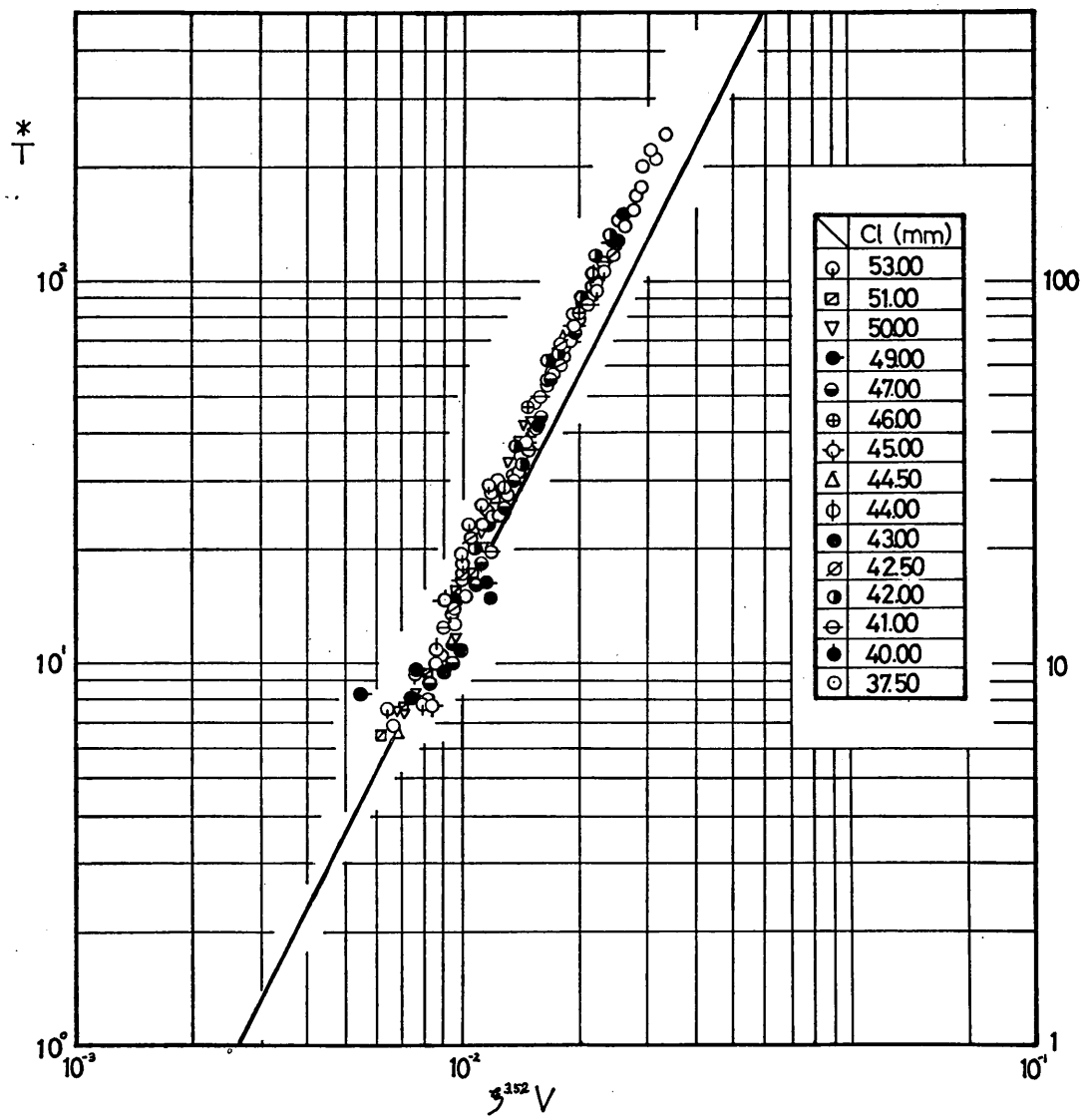

Fig. 4-4 Relationship between $\overset{*}{T}$ and $\xi^{3.52}\ V_p$

Now let us investigate this parameter by considering the experimental data. Since V_p required to same drag force changes inversely as the clearance C_L, a parameter for simslar flow can be obtained by selecting V_p and C_L for same $\overset{*}{T}$. Fig. 4-3 shows the relation between V_p and ξ for same value of $\overset{*}{T}$ in Fig. 4-2. We can findthat each point lays on the parallel lines for each $\overset{*}{T}$ on logarithmic graph paper.
From this result, the empirical formula

$$\xi^{3.52} V_p = C(\overset{*}{T}) \tag{49}$$

is derived. In equation (49), the right side is decided only by $\overset{*}{T}$.
Judging from this fact all data will be able to arrange so that they are independent for C_L using $\xi^{3.52} V_p$ and $\overset{*}{T}$.

Fig. 4-4 shows the relation between $\xi^{3.52} V_p$ and $\overset{*}{T}$. Though the drag force $\overset{*}{T}$ is not decided directly for ξ and V_p from this figure, it can be concluded that two kinds of flow with same $\xi^{3.52} V_p$ and different clearance give similar flow around the sphere.
Therefore, in equation (48) the relation between m and δ is given by

$$m = 3.52(2-\delta) \tag{50}$$

This suggests that the selection of dimensionless parameter from equation (47) is appropriate.

Now we consider drag coefficient C_D in equation (48).
Then C_D is expressed as follows:

$$C_D = \overset{*}{T} \Big/ \left(\frac{\rho}{2} D_s^2 V_p^2\right) = k_d \xi^m (\mu/\rho D_s V_p)^\delta$$
$$= k_d \xi^m R_D^\delta \tag{51}$$

where,

$$R_D = (\mu/\rho D_s V_p)$$

The drag coefficient $\overset{*}{C}_D$ is arrnged by Reynolds number and m given by equation (50). Now, if we use $\xi^{3.52} V_p$ in place of V_p in equation (51), $\overset{*}{C}_D$ is given as follows:

$$\overset{*}{C}_D = \overset{*}{T} \Big/ \left\{\frac{\rho}{2} (\xi^{3.52} V_p)^2 D_s^2\right\} = k_d' \{\mu/(\rho D_s \xi^{3.52} V_p)\}^\delta \tag{52}$$
$$= k_d' \overset{*}{R}_D^\delta$$

where,

$$\overset{*}{R}_D = \left(\frac{\mu}{\rho D_s \xi^{3.52} V_p}\right) \tag{53}$$

Fig. 4-5 shows the drag coefficient $\overset{*}{C}_D$ according to $\overset{*}{R}_D$. Though $\overset{*}{C}_D$ is almost constant in the region of relatively small $\overset{*}{R}_D$, it rises up with increase of $\overset{*}{R}_D$ and finally approaches to the constant value. This rising trend of $\overset{*}{C}_d$ can be considered as the result of abrupt change of the flow around back part of the sphere. The value of $\overset{*}{C}_D$,

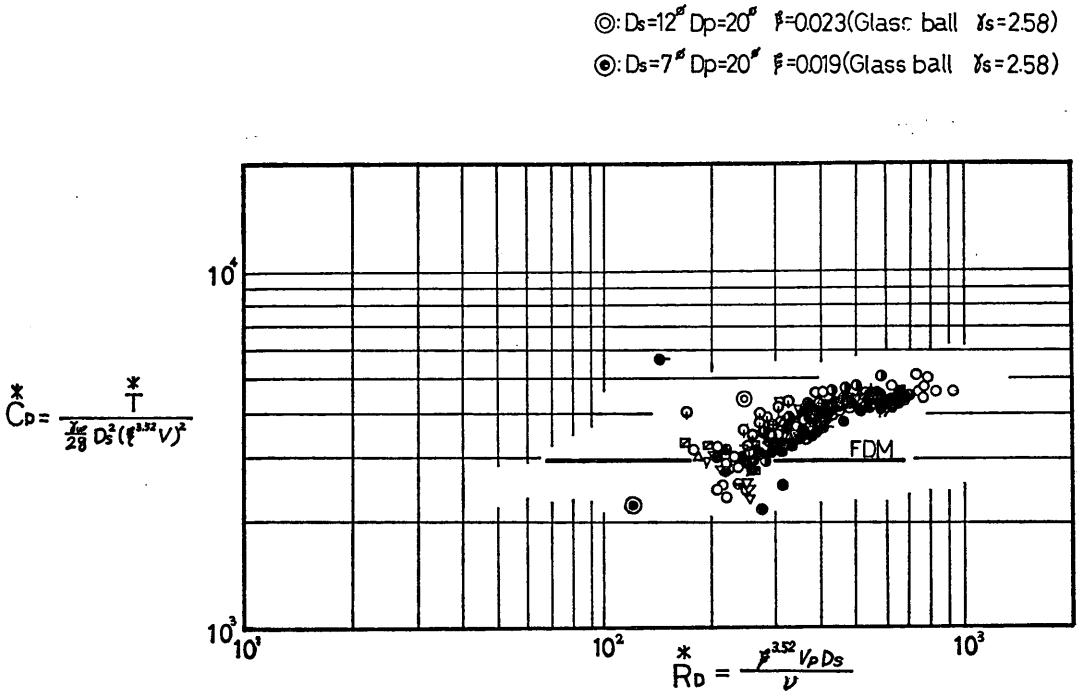

Fig. 4-5 Change of revised drag force according torevised Reynolds number

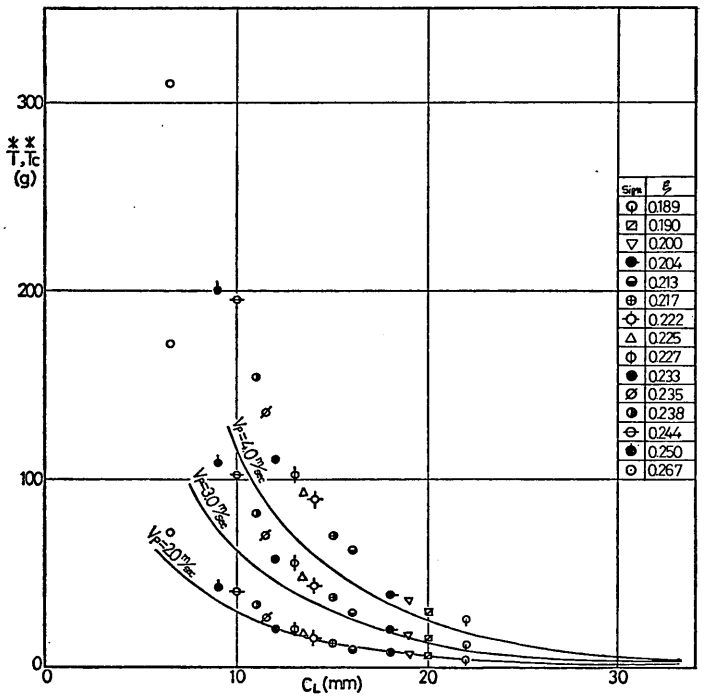

Fig. 4-6 Comparison of drag force between experiment and calculating results

or $\overset{*}{R}_D$, however, differs from C_D, or R_D in the order. This fact is caused by that $\xi^{3.52}V_p$ is not absolute velocity of the flow.

Even if the clearance differs, we assume that only one velocity distribution around the inlet of the suction pipe is given by the same drag force. And if we express the absolute velocity at arbitrary location by $V_{(r,z)}$, equation (54) is obtained.

$$V_{(r,z)}=K_{V(r,z)}\xi^{3.52}V_p \tag{54}$$

Though the constant $K_{V(r,z)}$ is obtained by using the calculated result in 4.2., this value varies to the location around the sphere. Therefore, it is no sense to decide this

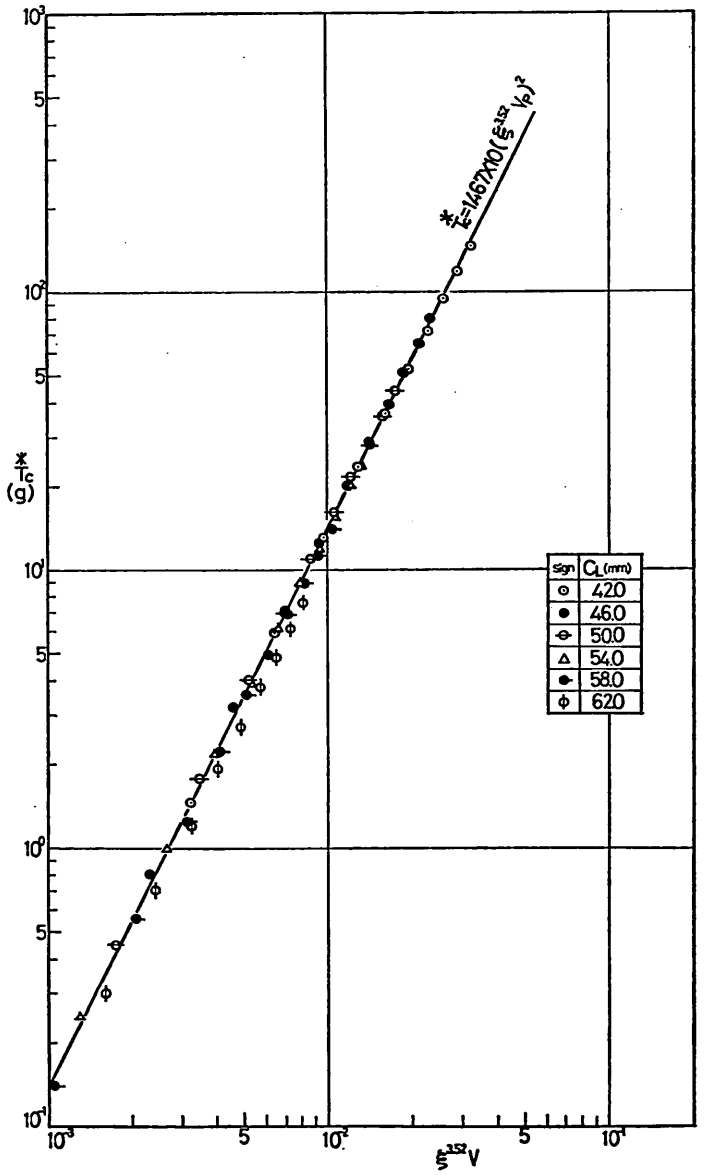

Fig. 4-7 Arrangement of calculating result by dimentionless parameter, $\xi^{3.52}$

value forcibly. But in the similar problems treated here it is useful to use $K_{V(r,z)}=1$.

4.2 Investigation for experimental results and calculation

By substituting $v_t=0$ into equation (44), T_C coincides buoyancy W_{VC} of the sphere. Therefore, $\overset{*}{T}_C$ expressed in equation (55) varies according to square of v_t.

$$\overset{*}{T}_C=T_C-W_{VC} \tag{55}$$

From equations (11) and (39),

$$v_t \propto V_p$$

Therefore, $\overset{*}{T}_C$ changes with square of V_p. This means that every value of $\overset{*}{T}_C$ for C_L can be obtained by the calculation on one set of $\overset{*}{T}_C$ and V_p. Thus, $\overset{*}{T}_C$ for each case of C_L was calculated and compared with experimental result $\overset{*}{T}$ as shown in Fig. 4-6. In this case $\overset{*}{T}_C$ is given by

$$\overset{*}{T}_C=A(\xi)\,V_p^2 \tag{56}$$

Though the difference between both results is small in the area of relatively large C_L, it increases as C_L decreases. This fact is due to that the calculation in this paper is for potential flow and, therefore, doesn't take account for the problems on separation and contraction effect at the end of suction mouth.

As far as the drag force of the sphere is concerned, this calculation cannot be adopted in the region in where the flow is under the control of separation and contraction. As such effects, however, affect only at the back part of the sphere, the flow at the remaining part may relatively close to potential flow. In order to verify this fact, there is necessary to compare the parameter $\xi^{3.52}$ derived from the experimental data with the calculated result.

$\overset{*}{T}_C$ for arbitrary V_p was calculated by equation (56) and these results were investigated by using dimensionless parameter $\xi^{3.52}$ in Fig. 4-7.
The result approximately lay on a straight line. From this figure, the approximate formula is obtained as followings.

$$\overset{*}{T}_C=1.467\times10^5(\xi^{3.52}V_p)^2 \tag{57}$$

$\overset{*}{C}_D$ and $\overset{*}{R}_D$ are given by equation (52) and (57) for the calculated result, which is the straight line in Fig. 4-5.

When we examine the value of $K_{V(r,z)}$ defined in equation (54), absolute velocity $V_{C(r,z)}$ on arbitrary point also arranged similarly by ξ as shown in Fig. 4-8. The absolute velocity is given from this figure as follows:

$$V_{C(r,z)}=K'_{V(r,z)}\cdot\xi^{3.35}V_p \tag{58}$$

In this case the exponent is 3.35, which somewhat differs from the exponent for $\overset{*}{T}_C$. This may come from the reason that the partition of the flow field near surface of the sphere is not consisted of square mesh. In accordance with the aforementioned consideration, it revealed that the calculated drag force has notable difference to that from experiment, but change of drag force and flow velocity around suction mouth with the clearance C_L are close to the result of the experiment. This fact means that the flow in the fairly wide area can be substituted by potential flow and suggests that the calculation presented in this paper is also useful in the examining similarlity for another formed suction mouth.

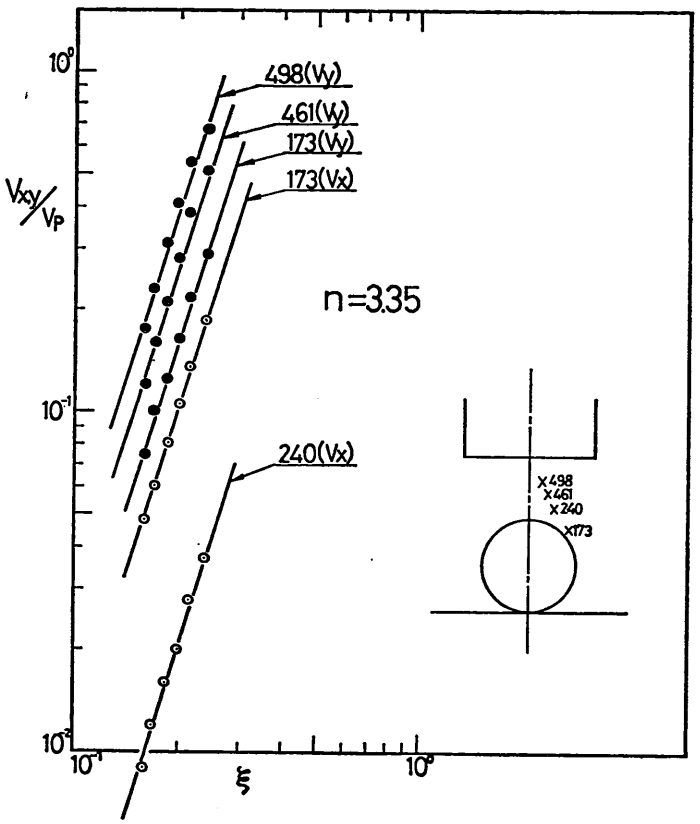

Fig. 4-8 Similarity of velocity at arbitrary location

4.3. Effect of contraction

In Fig. 4-5, $\overset{*}{C}_D$ calculated from the experimental data rises up hastily and approaches the constant value with the increase of $\overset{*}{R}_D$. Such a trend is different from the result for potential flow and is caused by the abrupt increase of velocity behind the sphere due to the separation and contraction effects. Generally speaking, drag coefficient on a sphere in uniform flow increases somewhat in the region $5\times10^3\leq R_e\leq10^4$ due to the transition of separation point in the laminar boundary layers.

Though Reynolds number which is equivalent to R_e cannot be decided in this paper, we can use R_{eD}, in which the representative velocity is indicated by v_m (Fig. 4-2) and the diameter of the sphere is adopted as representative length. In this experiment R_{eD} changes in the following region.

$$7\times10^3\leq R_{eD}\leq2.6\times10^4 \tag{59}$$

If R_{eD} is assumed to be close to R_e, this experiment was conducted in the region where separation point in laminar boundary layers changes. But in this experiment the flow around the sphere doesn't attain to the region where laminar boundary layers change to turbulent boundary layers and drag coefficient drops down abruptly.

However, the influence to drag coefficient by transition of separation point is a little. Therefore, the increase of the drag coefficient in Fig. 4-5 cannot be explained

only with separation on surface of the sphere. For this reason, in this paper, separation effect is ignored and the contraction effect at inlet of the suction mouth is only investigated.

Now let us assume that the drag force is close to that of potential flow for lower velocity or larger C_L. Then, the contraction doesn't exist and velocity at mouth inlet is V_p in Fig. 4-9.

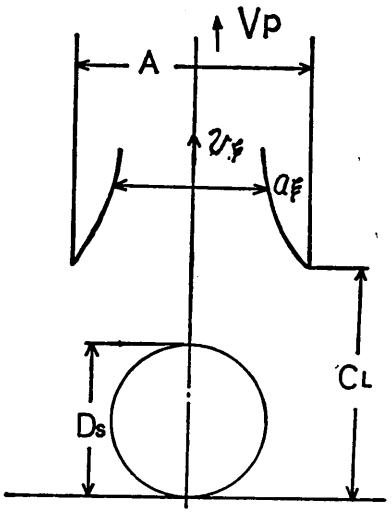

Fig. 4-9 Sketch of contracted inlet flow

By placing the bed closely toward the suction mouth or by increasing the flow velocity in pipe, the contraction due to the sphere and the clearance appears. In this time the cross setional area of contracted flow is expressed by a_ξ and the velocity by v_ξ. Further, if e_k is contraction coefficient given as

$$e_k=a_\xi/A \tag{60}$$

the amount of increasing velocity due to contraction, Δv, is given by

$$\begin{aligned}\Delta v&=v_\xi-V_p\\&=V_p\left(\frac{1}{e_k}-1\right)\end{aligned} \tag{61}$$

If the cross sectional area of the sphere for D_s is used as the area effected by Δv and ΔT is used as the amount of the increase of the drag force by contraction effect

$$\Delta T=\frac{\gamma_w}{2g}\Delta v^2 a_s^2 \tag{62}$$

is obtained. From equation (62) e_k is derived as follows:

$$e_k=\frac{1}{\left(\dfrac{8g\Delta T}{\pi\gamma_w V_p^2 D_s^2}\right)^{1/2}+1} \tag{63}$$

where,

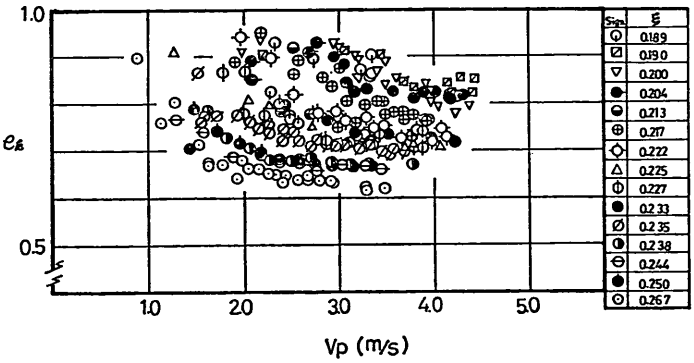

Fig.4-10 Contraction coefficient changed the approaching of a sphere and bed

$$\Delta T = \overset{*}{T} - \overset{*}{T}_C \tag{46}$$

Fig. 4-10 shows e_k according to V_p.

From this figure, we can find that there exist a little influence of velocity V_p and e_k approaches almost constant value. This constant value decreases with decrease of the clearance C_L and, that is, the influence of contraction effect increases.

A contraction coefficient is generally constant for turbulent flow and ranges from 0.6 to 1.0. Therefore, that contraction effect is distinguished as compared with separation effect may be the reasonable assumption. In the region of lower velocity, strong influence of V_p appears. It can be thought that this influence comes from the neglect of separation effect previously mentioned.

4.4. Application of parameter ξ^m to another problems

Equation (52) shows the relation derived by dimensional analysis and the experiment. Therefore, it can be applied theoretically for another case in which D_p or D_s differ from that in this paper. The applicability of equation (52) was also judged by the calculation to another experiment. This result is shown in Fig. 4-5. Though a few experiments on such a problem were conducted by another researcher and the example treated in this comparison are only two, these results for air lift pump with diameter of 20 mm coincide relatively to the result in this paper.

In the next place, let us consider the use of parameter ξ^m for drag head. Now we think the actual drag head equipped with teeth as a auxiliary dredging device. We select the diameter of suction pipe D_p, the mean velocity in the pipe V_p and the clearance between teeth and sea bed C_L as follows:

$D_p = 800$ mm
$V_p = 3.5$ m/s
$C_L = 100 \sim 105$ mm

When we plan to do model test for the actual drag head with aforementioned dimensions, the parameter ξ^m can be used. If $D_p' = 50$ mm as the pipe diameter and $V_p' = 3$ m/s as the velocity in suction pipe are used for the model drag head, $C_L' = 9$ mm is obtained from the relation (65).

$$\left(\frac{D_p'}{4C_L'}\right)^{3.52} V_p' = \left(\frac{D_p}{4C_L}\right)^{3.52} V_p \tag{65}$$

Finally we can obtain the similar flow for the actual drag head by selecting the clear-

ance of about 9 mm.

5. Conclusions

The drag force of the sphere on the model bed was measured to the various clearance between the suction mouth and the bed. And the numerical calculation by using Finite Difference Method was conducted for potential flow. The following matters were obtained as the results of this experiment and the numerical calculation.

(1) The similar flow when the solid body is sucked through the circular suction mouth and the clearance is varied cannot be given only by the horizontal mean inflow velocity v_m.

(2) By introducting the dimensionless parameter $\xi^{3.52}$ from the dimensional analysis concerning the drag force for a sphere, the relation (45) which gives the similar flow around suction mouth for different clearance is obtained.

If we use revised drag coefficient $\overset{*}{C}_D$ and revised Reynolds number $\overset{*}{R}_D$ which involve the parameter $\xi^{3.52}$, $\overset{*}{C}_D$ is expressed only by the function of $\overset{*}{R}_D$. Then $\overset{*}{C}_D$ increases gradually with increase of $\overset{*}{R}_D$ and finally approaches to the constant value. In this experiment

$$2.5\times10^3\leq\overset{*}{C}_D\leq5\times10^3 \quad \text{for } 1.8\times10^2\leq\overset{*}{R}_D\leq10^3$$

(3) The drag force was calculated numerically by using Finite Difference Method under the assumption of axially symmetric and potential flow. Consequently, though the calculated drag force closes to the experimental result for $\overset{*}{R}_D\leq200$, the difference between two values from the experiment and calculation expands as $\overset{*}{R}_D$ increases. It is clarified that this fact mainly depends on the increase of velocity behind the sphere due to contraction effect. The drag force calculated, however, is also arranged by using $\xi^{3.52}V_p$ for the various clearance C_L and is expressed approximately by equation (57). Further, the absolute velocity $V_{C(r,z)}$ at arbitrary location is expressed as

$$V_{C(r,z)}=K'_V\xi^{3.35}V_p$$

The exponent of this equation is close to 3.52.

(4) The influence by contraction effect was investigated by using the difference between the experimental and calculated results for potential flow. It was clarified that the contract coefficient e_k has strong influence to the drag force to the sphere approaching toward the suction mouth and has constant value for comparatively high V_p.

(5) The applicability of equation (52) for another experiments was deliberated. In consequence of this comparison, these results coincide relatively to the result presented in this paper.

(6) The similarlity parameter for suction mouth is not always applied to another problems on a lift by mouth piece with complicated shape, but this may undoubtedly present valuable data for the problems related to how a lift is changed by clearance.

(7) The numerical calculation for potential flow is not useful especially obtaining drag force on the dull-shaped solid body. It, however, is very convenient method in determining of the similarity and the change of flow for some kinds of complicated -shaped mouth piece and various clearance.

As shown in the investigation of contract phenomenon, the problems of vortex formation and separation are not ignored around the area in where flow velocity is

relatively low. These problems must be further investigated by means of the measuring back pressure of the sphere.

Further it is scheduled that the application of the similarity parameter for different suction pipes and prheres will be conducted from now on in the experiment concerning the lift by air-lift suction mouth.

6. Acknowledgements

In the analysis of this paper the precious opinion was given by Mr. Koreishi and Mr. Hamada, members of the Hydraulic Transportation Laboratory.

We express our heartfelt thanks to them.

(Received 30 June 1975)

Appendix I. Notation

The following symbols have been used in this paper:

a_s =projected area of a sphere;
A =cross-sectional area;
a_ξ =cross-sectional area of contracted flow;
C_D =drag coefficient;
$\overset{*}{C}_D$ =revised drag coefficient;
C_L =clearance between bed and suction mouth;
D_s =sphere diameter;
D_p =pipe diameter;
e_k =contract coefficient;
H_w =water level of water pool;
i =number of cross point in the partitioned flow field;
j =number of calculation by gradual equation;
n =number of calculation by gradual equition, also length in normal;
p_s =pressure on the sphere surface;
r =horizonat axis in flow field;
R_e =Reynolds number of a sphere laid in uniform flow;
R_{eD} =equivalent Reynolds number;
$\overset{*}{R}_D$ =revised Reynolds number;
T =tension of the spheremeasured in this experiment;
$\overset{*}{T}$ =drag force in the experiment;
$\overset{*}{T}_C$ =drag force given by the calculation;
u =velocity component in r-axis;
V_p =mean velocity in suction pipe;
v_m =horizontal mean velocity of inlet flow;
v_t =tangential velocity on a sphere;
v_ξ =velocity of contracted flow;
$V_{(r,z)}$ =absolute velocity at arbitrary location (r, z);
w =velocity component in z-axis;
Z =vertical axis;
ε_r =error of the calculating result against basic equation by finite difference method;
ε_n =finish error in calculation;

ξ =dimensionless parameter;
Δ =space of mesh;
γ_w =specific weight of water;
ρ =density;
μ =absolute viscosity;
ν =kinematic viscosity;
ψ =Stockes' stream function;

Appendix II. Reference

1) T. Yagi, Y. Okayama, et al., "Dredging Effects of Water Jets and Teeth equipped with the Trailing Suction Head of the Tokushun-maru No. 1," Technical Note of P.H.R.I., No. 141, 1972.
2) M. Kondo, T. Yagi, Y. Okayama, et al., "Dredging Efficiency and Power Consumption of the Tokushun-maru No. 1. at time of dredging the hard packed sand," Technical Note of P.H.R.I., No. 168, 1973.
3) "Fluid mechanics", Victor L. Streeter, McGraw-Hill Book Company.
4) Jiro Kondo, "Applied Mathematics (the last volume),", Maruzen Press Inc.
5) Y. Kato, T. Iwasaki, "Study on Air lift Pump for solid particles, "Transaction of JSME, 48th National Convention, No. 700-15, pp. 13 16, 1970.